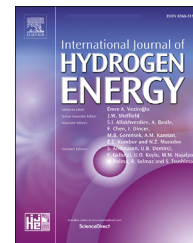




ELSEVIER

Available online at [www.sciencedirect.com](http://www.sciencedirect.com)

ScienceDirect

journal homepage: [www.elsevier.com/locate/he](http://www.elsevier.com/locate/he)

# Non-noble metallic nanoparticles supported on titania spheres as catalysts for hydrogen generation from hydrolysis of ammonia borane under ultraviolet light irradiation

X.J. Yang<sup>\*</sup>, C.Y. Wang, R.Y. Gao, Z.M. Lu, X.H. Zhang, X.F. Yu, L.L. Li<sup>\*\*</sup>

School of Materials Science and Engineering, Hebei University of Technology, Tianjin, 300130, PR China

## ARTICLE INFO

### Article history:

Received 16 May 2018

Received in revised form

3 July 2018

Accepted 9 July 2018

Available online xxx

### Keywords:

Ammonia borane

Hydrolysis

Non-noble metallic nanoparticles

Titania spheres

Ultraviolet light irradiation

## ABSTRACT

Herein, a report on non-noble metal (Ni, Co, Cu, and their combination) nanoparticles (NPs) supported on TiO<sub>2</sub> spheres as catalysts for hydrogen generation via hydrolysis of ammonia borane (NH<sub>3</sub>BH<sub>3</sub>, AB) is provided. The TiO<sub>2</sub> spheres were prepared through a template method by using polystyrene (PS). The metallic nanoparticles were synthesized by a redox replacement reaction. The structure, morphology, and chemical composition of the obtained samples were analyzed by X-ray diffraction (XRD), scanning electron microscopy (SEM), transmission electron microscopy (TEM) equipped with energy dispersive X-ray spectroscopy (EDX), and X-ray Photoelectron Spectroscopy (XPS). The characterization results showed that the metallic nanoparticles were well dispersed on the TiO<sub>2</sub> supports. The catalytic activity toward the hydrolysis of AB was found to correlate well with the amount of metallic elements in catalysts while for the multicomponent phases, a synergistic effect was noticed. Theoretical calculations revealed that Ni, Co, and Cu atoms significantly influenced the electronic behavior of TiO<sub>2</sub> and thereby, the catalytic properties of the materials.

© 2018 Hydrogen Energy Publications LLC. Published by Elsevier Ltd. All rights reserved.

## Introduction

Hydrogen is known as a clean and renewable energy carrier, properties which recommend it as a suitable and efficient alternative to the fossil fuel feedstocks [1,2]. Ammonia borane (NH<sub>3</sub>BH<sub>3</sub>, AB) has 6H atoms in the molecule, which is equivalent with a hydrogen content of 19.6 wt%. The hydrogen content of AB exceeds that of many compounds used to generate hydrogen via hydrolysis, such as borohydrides (LiBH<sub>4</sub>

– 18.3 wt%, NaBH<sub>4</sub> – 10.8 wt%) and metal hydrides (e.g., MgH<sub>2</sub>, 7.7 wt% and Mg<sub>3</sub>La, ca. 7.7 wt%). In addition, AB has high chemical stability at room temperature compared to borohydrides [3]. Therefore, AB is considered as an attractive source of hydrogen for fuel cells, because it combines both chemical hydrogen storage and production due to its high hydrogen content and stability at room temperature, conditions in which the fuel cell operates. AB can release hydrogen by pyrolysis or hydrolysis with a suitable catalyst. The pyrolysis reaction is not very convenient, because it takes place at high

<sup>\*</sup> Corresponding author.

<sup>\*\*</sup> Corresponding author.

E-mail addresses: [yangxiaoqing@hebut.edu.cn](mailto:yangxiaoqing@hebut.edu.cn) (X.J. Yang), [Liabc@hebut.edu.cn](mailto:Liabc@hebut.edu.cn) (L.L. Li).

<https://doi.org/10.1016/j.ijhydene.2018.07.049>

0360-3199/© 2018 Hydrogen Energy Publications LLC. Published by Elsevier Ltd. All rights reserved.

temperature, which is not suitable for the fuel cell, while generates toxic byproducts [4]. AB completely decomposes at high temperatures during pyrolysis, so the power consumption does not meet the recent targets imposed by the environmental legislation [5,6]. During the last years, the ionic liquids have been reported to be an appropriate solution to increase the amount of hydrogen released from AB. In this case, the AB is introduced in the ionic liquid that attacks the AB molecule bonds releasing hydrogen [7]. However, the reported ionic liquids are usually complicated organic salts, which are not easy to prepare and not environmentally preferred.

Nowadays, the hydrolysis of AB is accomplished by using metal catalysts, such as Pt, Rh, and Ru [8–10]. Due to the high costs of these noble metals, researchers have recently begun to seek the non-noble metals, which are cost-effective and show relatively high catalytic activity, especially when they are used as nanoparticles whose size is small enough to enhance their catalytic performance [11–13]. Therefore, a tendency to use non-noble metals for the hydrolysis of AB was observed lately. As a result, the cost of the overall process of hydrogen release was reduced due to the practical use [14,15]. Since the monometallic NPs usually manifest poor performance, trimetallic NPs can be considered as better catalysts with enhanced catalytic performance rationalized by the synergistic effect between the neighboring elements in the same NP. In this sense, a large number of studies focused on the catalysts of Cu combined with other metallic nanoparticles for AB hydrolysis. Wang et al. synthesized trimetallic magnetic Cu@FeNi core-shell NPs, which are composed of crystalline Cu cores and amorphous FeNi shells [16]. Cu@FeCo and Cu@CoNi manifested composition dependent activities towards the hydrolysis of AB [17]. Moreover, core-shell structured trimetallic NPs Cu@CoCr and Cu@CoW were synthesized using one-step in-situ synthesis method and evaluated in the hydrolysis of AB [18]. However, these nanoparticles can form large aggregates, whose catalytic activity is reduced accordingly. An efficient strategy to improve their stability consists of loading these nanoparticles on an inorganic support, when the interaction established between the NPs and support surface will stabilize them and thus, the agglomeration will be prevented while the catalytic behavior will be improved.

TiO<sub>2</sub> is a well-known photocatalyst for many chemical reactions due to its chemical inertness, cost-effective, and long-term stability against chemical-corrosion [19]. Moreover, it can be used as a suitable support for functional materials. Murat Rakap et al. loaded Pd on TiO<sub>2</sub> NPs, and the resulted material was found to be highly active and reusable in the hydrolysis of AB, even at low temperature and concentration [20]. Recently, the incorporation of metal within TiO<sub>2</sub> has been shown to be a good strategy to produce excellent photocatalysts toward hydrogen release from AB [21–23]. The metallic catalysts supported on TiO<sub>2</sub> showed strong metal-support interaction (SMSI), an effect that highly increases the catalytic activity. The high photocatalytic activity is explained by the good separation of electrons and holes. However, all the TiO<sub>2</sub> used as supports were nanofibers synthesized by electrospun method. Therefore, other methods to prepare TiO<sub>2</sub> support with different morphologies

are highly encouraged, especially since the morphology of the support can play a significant role in the dispersion of the active phase, which is intimately related to the catalytic performance.

In this study, Ni<sub>0.3</sub>Co<sub>0.3</sub>Cu<sub>0.4</sub> NPs were synthesized through a redox replacement reaction using TiO<sub>2</sub> spheres as a support. The TiO<sub>2</sub> spheres display high surface area on which the tri-component Ni<sub>0.3</sub>Co<sub>0.3</sub>Cu<sub>0.4</sub> NPs can be uniformly dispersed. The as-prepared Ni<sub>0.3</sub>Co<sub>0.3</sub>Cu<sub>0.4</sub>/TiO<sub>2</sub> catalysts exhibited promising catalytic activities toward the hydrolysis of AB under ultraviolet light (UV-light) irradiation. Theoretical calculations were carried out aiming to study the changes in the electronic properties of the reaction system, which cause the SMSI effect, and to confirm the effect of TiO<sub>2</sub> on the catalytic activity of Ni<sub>0.3</sub>Co<sub>0.3</sub>Cu<sub>0.4</sub>.

## Experimental

### Preparation of polystyrene (PS) spheres

The monodisperse PS spheres were prepared by emulsifier-free emulsion polymerization according to reference [24]. In a typical synthesis, 10.0 g of styrene, 1.5 g of poly (vinyl pyrrolidone) (PVP) K30 (Mw ≈ 40000), 0.26 g of cationic initiator 2, 2'-azobis-(isobutyramidine) dihydrochloride (AIBA), and 100.0 g of distilled water were loaded into a 250 mL three-neck flask equipped with a mechanical stirrer, a thermometer with a temperature controller, a N<sub>2</sub> inlet, a Graham condenser, and a heating oil bath. The air in the flask was removed from the reaction solution by bubbling N<sub>2</sub> at room temperature for 90 min. Then, the reaction was performed at 343 K for 24 h under a stirring rate of 150 rpm. The obtained PS suspension was centrifuged (6000 rpm, 5 min), washed in ethyl alcohol for at least three times, and the content of PS suspension was then washed by ethanol.

### Preparation of catalysts

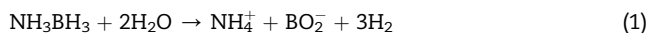
0.03 g of Ni(NO<sub>3</sub>)<sub>2</sub>·6H<sub>2</sub>O (99%), Co(NO<sub>3</sub>)<sub>2</sub>·6H<sub>2</sub>O (99%), or Cu(NO<sub>3</sub>)<sub>2</sub>·6H<sub>2</sub>O (99%), 12–36 mL of 28 wt% aqueous ammonia solution, and 160 mL of ethyl alcohol were added into 20.0 g of the PS suspension. The sol-gel reaction was carried out at 323 K for 1.5 h, and the metal composite spheres (M/TiO<sub>2</sub>, M = Ni, Co, Cu or their compounds) were obtained. After drying in a vacuum oven at 323 K overnight, the resulted fine powders were used as catalysts.

### Catalysts characterization

The as-synthesized catalysts were characterized by powder X-ray diffraction (XRD, Rigaku D/max-2500 X-ray generator, Cu Kα radiation), scanning electron microscopy (SEM, JEOL JSM6700F), inductively coupled plasma emission spectroscopy (ICP-9000, Thermo Jarrell-Ash Corp.), transmission electron microscopy coupled with energy dispersive X-ray spectroscopy (TEM and EDX, Philips Tecna F20, 200 kV), X-ray photoelectron spectroscopy (XPS, ESCALAB 250Xi), and UV-Vis diffuse reflectance spectroscopy (DR UV-Vis, Hitachi U-3900H).

## Dehydrogenation of AB

In a typical experiment, AB solution was placed in a sealed 50 mL flask fitted with an outlet tube for collecting the released  $H_2$ . The outlet tube was connected to a micro gas flowmeter (RTK-GMA-II) to record the released  $H_2$  volume necessary to calculate the rate. A certain amount of catalyst was added into the AB solution under soft stirring. AB hydrolysis reaction was proceeded as soon as the catalyst was added at 25–40 °C. The process of AB hydrolysis was described as follows [25].



When the AB hydrolysis was completed, the residual solution was centrifuged (6000 rpm, 15 min) and washed, then the catalyst was recycled.

## Computational methods

All the calculations were processed using the density functional theory (DFT) method using the DMol<sup>3</sup> code [26]. The generalized gradient approximation was carried out by combining the PerdewWang correlation functional with the Becke exchange functional [27].  $TiO_2$  anatase phase was considered for the calculation model. Self-consistent field calculations were carried out with a convergence criterion of  $10^{-6}$  a.u. for the total energy. We considered M (M = Ni, Co, Cu) loading effects using  $2 \times 2 \times 1$  supercell. One M atom was filled in the exterior position of  $TiO_2$ .  $5 \times 5 \times 1$  MonkhorstePack k-points meshes were used for structural optimization, and  $3 \times 4 \times 1$  k-points were conducted for electronic structure calculations. The adsorption energy ( $E_{ads}$ ) was obtained from the following expression.

$$E_{ads} = E(M/TiO_2) - E(TiO_2) - E(M) \quad (2)$$

where  $E(M/TiO_2)$ ,  $E(TiO_2)$ , and  $E(M)$  are representative of the total energies for the metal-loaded on  $TiO_2$ , the pristine  $TiO_2$ , and bare metal, respectively. Thus,  $E_{ads} < 0$  corresponds to an exothermic adsorption leading to the minimum stable toward dissociation.

## Results and discussion

### Physico-chemical properties of the samples

Fig. 1 shows the XRD patterns of the  $TiO_2$  sphere and metallic NPs supported on  $TiO_2$ . It can be observed that the diffractogram of  $TiO_2$  (Fig. 1a) display one broadened diffraction peak at about  $2\theta = 25.3^\circ$  (marked by the triangle signal), corresponding to anatase phase (JCPDS No. 1–562). The absence of any other diffraction peaks stands for the amorphous structure of the support. The diffraction pattern for the metal supported NPs on  $TiO_2$  (Fig. 1b) exhibits another obvious peak at  $2\theta = 44.0^\circ$  (marked by a filled circle), which is ascribed to the metal phase (the peak of Ni and Co are at about  $2\theta = 44.5^\circ$ , the peak of Cu is at about  $2\theta = 43.5^\circ$ ) in the sample. It is sharp may due to the affect of the noise for the poor crystallinity. The

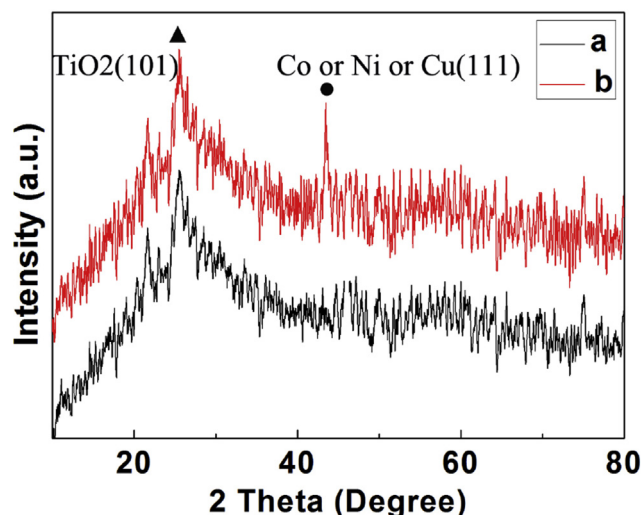
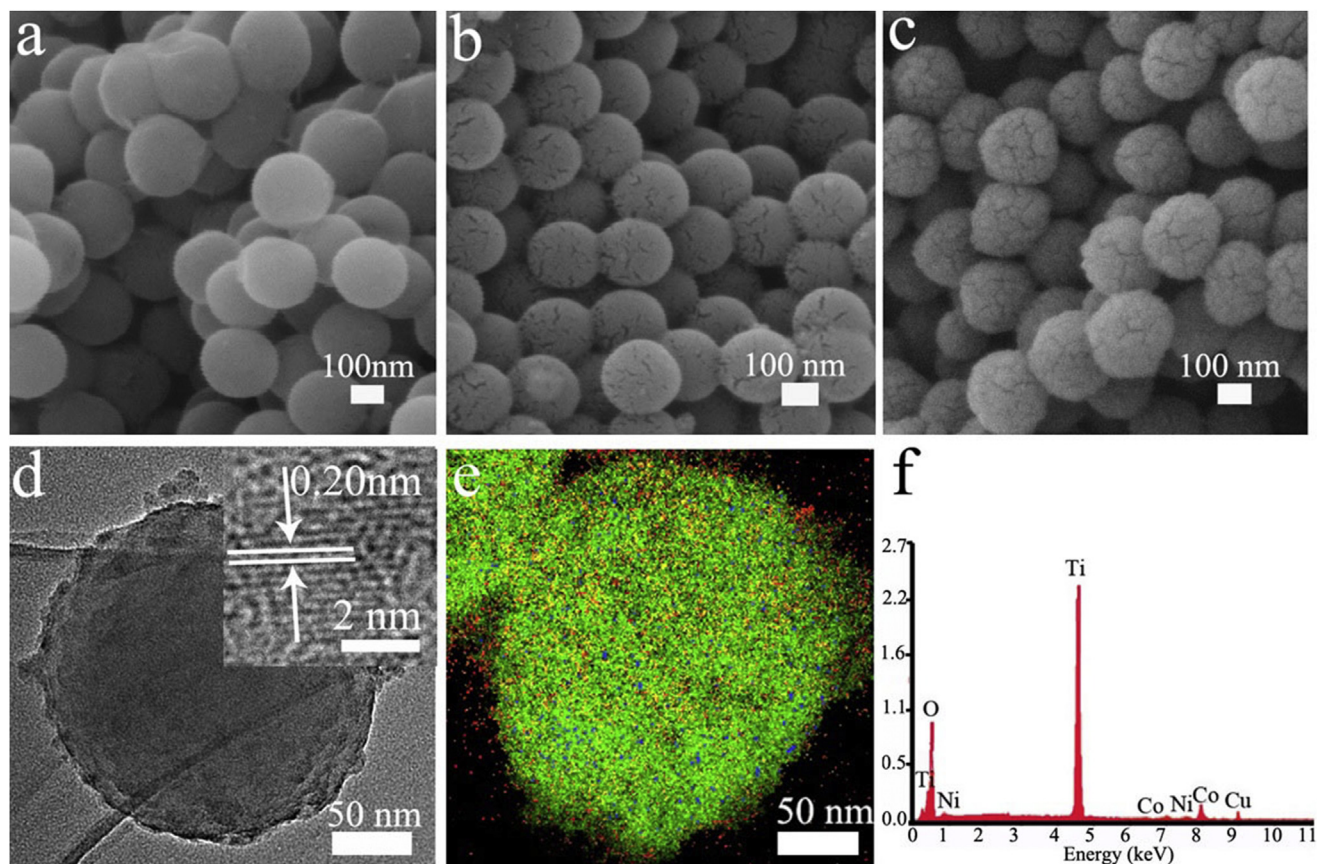


Fig. 1 – XRD patterns of catalysts. (a)  $TiO_2$ , (b)  $Ni_{0.3}Co_{0.3}Cu_{0.4}/TiO_2$  (10 wt% metal loading).

crystallization of metal phase was not high, because of the low reaction temperatures used during preparation of the sample. Thus, only one distinct peak indexed to metal phase was detected, which can be explained by the small size of the NPs that are highly dispersed on the solid support. Indeed, when Ni, Cu, and Co are loaded on a reducible support like  $TiO_2$ , they can be easily prepared as highly dispersed and stable NPs as a result of the support–metal interactions that are strong. However, it is difficult to determine whether our CuCoNi samples are presented as a compound or simply a physical mixture based on their XRD patterns. Hence, the formation of the CuCoNi compound cannot be confirmed beyond a doubt by the XRD results alone. ICP elemental analysis of the synthesized samples was performed to determine the exact composition of Ni, Co, and Cu in the catalysts. The obtained values, expressed herein as molar ratio, Ni:Co:Cu = 0.3:0.3:0.4. The initial raw materials ratio (molar ratio of  $Ni(NO_3)_2 \cdot 6H_2O:Co(NO_3)_2 \cdot 6H_2O:Cu(NO_3)_2 \cdot 6H_2O$ ) of 1:1:2 finally led to  $Ni_{0.3}Co_{0.3}Cu_{0.4}$ .

The morphology and composition  $Ni_{0.3}Co_{0.3}Cu_{0.4}/TiO_2$  of the obtained products were investigated by SEM, TEM, and EDX. Fig. 2a–c show the typical SEM images of the pure  $TiO_2$  sphere (Fig. 2a) and metal supported on  $TiO_2$  before and after reaction (Fig. 2b and c). The diameters of  $TiO_2$  spheres and metal supported  $TiO_2$  are about 150–200 nm. The surface of pure  $TiO_2$  is smooth, while the surfaces become rough and some cracks appear after loading the metal phases. Moreover, the cracks become larger after the catalytic reaction, as shown in Fig. 2c. It seems that these cracks are responsible for the decreasing of the hydrolysis rate during the recyclability tests. Fig. 2d displays the typical TEM images of the supported catalysts. To note, the metal particles are well dispersed on the  $TiO_2$  surface without any obvious agglomeration. Thus, the metal particles are well distributed of the spheres surface with diameter ranging from 5 to 10 nm (Fig. 2f). Elemental mapping was performed to see the element distribution. In Fig. 2e, the green, red, and yellow dots stand for Cu, Co, and Ni elements, respectively. Therefore, it can be stated that the metal



**Fig. 2** – SEM images of  $\text{Ni}_{0.3}\text{Co}_{0.3}\text{Cu}_{0.4}/\text{TiO}_2$  (10 wt% metal loading) before (a) and after reaction (b), and after 5 cycles of reaction (c). TEM image of fresh  $\text{Ni}_{0.3}\text{Co}_{0.3}\text{Cu}_{0.4}/\text{TiO}_2$  (10 wt% metal loading) (d). Cu, Ni, Co elemental mapping of  $\text{Ni}_{0.3}\text{Co}_{0.3}\text{Cu}_{0.4}/\text{TiO}_2$  sphere with 10 wt% metal loading (e). The EDS spectra of  $\text{Ni}_{0.3}\text{Co}_{0.3}\text{Cu}_{0.4}/\text{TiO}_2$  catalyst (f).

elements are well distributed on  $\text{TiO}_2$  spheres, without any evidence of aggregation. As can be seen, elements of Cu, Ni and Co are homogeneously distributed in the spheres, demonstrating that our sample is the CuCoNi compound rather than the mixture of Cu, Co and Ni [28]. The composition of the samples was determined by the EDX analysis, and the results are shown in Fig. 2f. The EDX spectra confirms the presence of Ti, Ni, Co, and Cu, while the total metal amount (Ni, Co, and Cu) is 10 wt%. Hence, according to EDX results showing Ni, Cu, and Co in the same particle, it could be affirmed that the metal nanoparticles are as CuCoNi alloy.

XPS was performed to determine the chemical composition of the catalyst surface and oxidation state of the elements. The high resolution spectra of Ni 2p, Co 2p, and Cu 2p showing the peak resolving and fitting for each element in  $\text{Ni}_{0.3}\text{Co}_{0.3}\text{Cu}_{0.4}$  sample are displayed in Fig. 3. The XPS results for Ni 2p (Fig. 3a) show that the binding energies at 852.3 and 869.7 eV correspond to Ni 2p<sub>3/2</sub> and Ni 2p<sub>1/2</sub>, respectively. Fig. 3b shows the high resolution XPS spectrum of Co 2p. The peaks at 780.8 and 796.9 eV correspond to Co 2p<sub>3/2</sub> and Co 2p<sub>1/2</sub>, respectively. According to these values, metallic and cationic species of the elements coexist in the sample. It is assumed that the small size of the NPs could easily cause the oxidation of metallic nickel and cobalt. The deconvolution of the Cu 2p spectrum is shown in Fig. 3c. The peaks at 932.2 and 954.5 eV are associated with Cu 2p<sub>2/3</sub> and Cu 2p<sub>1/2</sub>,

respectively, while the other peaks are assigned to copper in copper oxide. The appearance of cobalt, nickel, and copper oxides is inevitable, and this can be attributed to the exposure of samples to oxygen before and during the XPS.

The optical properties of the samples were analyzed by UV-vis diffuse reflectance spectroscopy (DR UV-Vis). The recorded spectra are shown in Fig. 4A, and they provided additional evidence for the property of light absorption of  $\text{TiO}_2$  that can be finely tuned by the introduction of different metal when the generated SMSI plays a key role in the photoresponse. In particular, the loading of metals on  $\text{TiO}_2$  is able to extend its light absorption to the visible region. Thus, the metal loaded on  $\text{TiO}_2$  can be photoexcited by the irradiation under visible light and probably could exhibit the photocatalytic performance of  $\text{TiO}_2$  for certain reactions. The absorption edges of  $\text{TiO}_2$ , Ni/ $\text{TiO}_2$ , Co/ $\text{TiO}_2$ , Cu/ $\text{TiO}_2$ ,  $\text{Ni}_x\text{Co}_y/\text{TiO}_2$  (The feed molar ratio of x:y = 1:2, denoted as  $\text{Ni}_1\text{Co}_2$ , the following are the same),  $\text{Ni}_1\text{Cu}_2/\text{TiO}_2$ ,  $\text{Co}_1\text{Cu}_2/\text{TiO}_2$ , and  $\text{Ni}_{0.3}\text{Co}_{0.3}\text{Cu}_{0.4}/\text{TiO}_2$  are determined to be about 353, 348, 350, 340, 348, 345, 345, and 310 nm, respectively. A plot obtained via the transformation based on the Kubelka-Munk (KM) function versus the energy of light is shown in Fig. 4B, by which the roughly estimated band gap values are 3.60, 3.35, 3.45, 3.10, 3.30, 3.25, 3.25, and 3.00 eV and correspond to  $\text{TiO}_2$ , Ni/ $\text{TiO}_2$ , Co/ $\text{TiO}_2$ , Cu/ $\text{TiO}_2$ ,  $\text{Ni}_1\text{Co}_2/\text{TiO}_2$ ,  $\text{Ni}_1\text{Cu}_2/\text{TiO}_2$ ,  $\text{Co}_1\text{Cu}_2/\text{TiO}_2$ , and  $\text{Ni}_{0.3}\text{Co}_{0.3}\text{Cu}_{0.4}/\text{TiO}_2$ , respectively. These results indicate a band gap

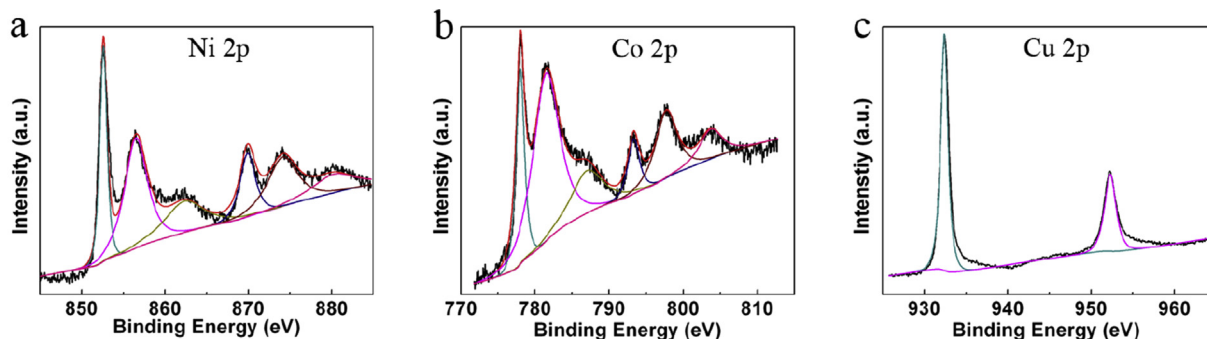


Fig. 3 – High resolution Ni 2p (a), Co 2p (b), and Cu 2p (c) XPS spectra of  $\text{Ni}_{0.3}\text{Co}_{0.3}\text{Cu}_{0.4}/\text{TiO}_2$ .

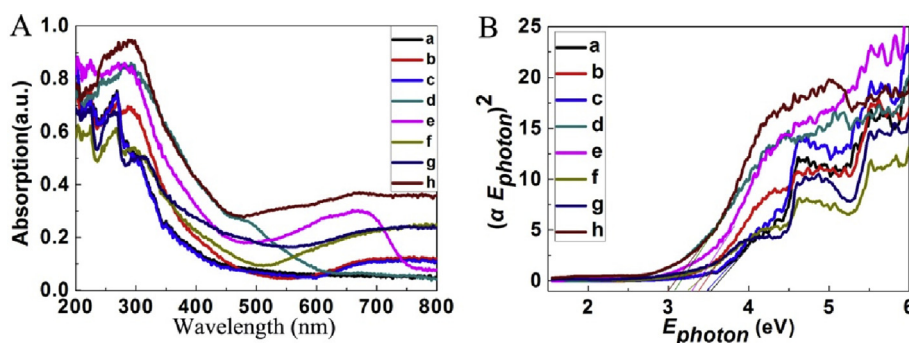


Fig. 4 – The DR UV–vis absorption spectra (A) and Tauc's plot for band gap energy determination (B) of the prepared samples. (a)  $\text{TiO}_2$ , (b)  $\text{Ni}/\text{TiO}_2$ , (c)  $\text{Co}/\text{TiO}_2$ , (d)  $\text{Cu}/\text{TiO}_2$ , (e)  $\text{Ni}_1\text{Co}_2/\text{TiO}_2$ , (f)  $\text{Ni}_1\text{Cu}_2/\text{TiO}_2$ , (g)  $\text{Co}_1\text{Cu}_2/\text{TiO}_2$ , and (h)  $\text{Ni}_{0.3}\text{Co}_{0.3}\text{Cu}_{0.4}/\text{TiO}_2$ .

narrowing for the metal loaded on  $\text{TiO}_2$ , as compared to unloaded  $\text{TiO}_2$ , which could be attributed to the formation of impurity energy levels of loaded metal ions between the valence band and conduction band of  $\text{TiO}_2$ .

### Catalytic activity

The catalytic activity of the synthesized catalysts in the hydrolysis of AB solution was investigated. The catalytic performances of the prepared  $\text{TiO}_2$  and metal supported  $\text{TiO}_2$  without light irradiation have been evaluated. Fig. 5 shows the  $\text{H}_2$  volume generated as a function of time for a 10 mL AB (0.023 g) solution and 5 mg of catalyst. The synthesized  $\text{TiO}_2$

spheres exhibit no catalytic activity during the hydrolysis of AB, while the release of hydrogen was obviously noticed when the metallic NPs (Ni, Co, Cu, or their combination) loaded on  $\text{TiO}_2$  were used, signifying their favorable catalytic activities. The hydrolysis reaction of AB over the as-synthesized metallic NPs supported on  $\text{TiO}_2$  without light irradiation is completed in approximately 30–40 min. The as-synthesized  $\text{Ni}_{0.3}\text{Co}_{0.3}\text{Cu}_{0.4}/\text{TiO}_2$  displays the highest catalytic activity, the reaction being completed in 15 min. At the end of the reaction, the calculated molar ratio of the generated  $\text{H}_2$  to the initial AB was approximately 3.0.

With the molar ratio of Cu changing, the  $\text{Ni}_x\text{Co}_y\text{Cu}_{1-x-y}/\text{TiO}_2$  catalysts exhibited different catalytic performances (Fig. 5)

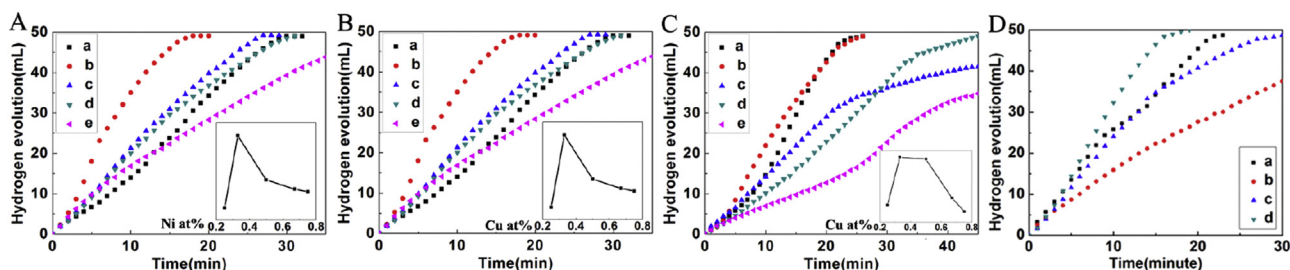


Fig. 5 – Hydrogen evolution without light assistance with different catalysts and using 0.023 g AB solution. A -  $\text{Ni}_x\text{Co}_y/\text{TiO}_2$  with different Ni: Co ratios, x: y, i.e., 1: 3 (a), 1: 2 (b), 1: 1 (c), 2: 1 (d), 3: 1 (e) (Denoted as  $\text{Ni}_1\text{Co}_3/\text{TiO}_2$ ,  $\text{Ni}_1\text{Co}_2/\text{TiO}_2$ ,  $\text{Ni}_1\text{Co}_1/\text{TiO}_2$ ,  $\text{Ni}_2\text{Co}_1/\text{TiO}_2$ ,  $\text{Ni}_3\text{Co}_1/\text{TiO}_2$ ). B -  $\text{Ni}_1\text{Cu}_3/\text{TiO}_2$  (a),  $\text{Ni}_1\text{Cu}_2/\text{TiO}_2$  (b),  $\text{Ni}_1\text{Cu}_1/\text{TiO}_2$  (c),  $\text{Ni}_2\text{Cu}_1/\text{TiO}_2$  (d),  $\text{Ni}_3\text{Cu}_1/\text{TiO}_2$  (e). C -  $\text{Co}_1\text{Cu}_3/\text{TiO}_2$  (a),  $\text{Co}_1\text{Cu}_2/\text{TiO}_2$  (b),  $\text{Co}_1\text{Cu}_1/\text{TiO}_2$  (c),  $\text{Co}_2\text{Cu}_1/\text{TiO}_2$  (d),  $\text{Co}_3\text{Cu}_1/\text{TiO}_2$  (e). D -  $\text{Ni}_1\text{Co}_1\text{Cu}_1/\text{TiO}_2$  (a),  $\text{Ni}_2\text{Co}_1\text{Cu}_1/\text{TiO}_2$  (b),  $\text{Ni}_1\text{Co}_2\text{Cu}_1/\text{TiO}_2$  (c),  $\text{Ni}_1\text{Co}_1\text{Cu}_2/\text{TiO}_2$  (d).

**Table 1** – The hydrogen generation rates of the AB hydrolysis over M/TiO<sub>2</sub> catalysts without light assistance.

Catalyst (Initial raw material rate)	The rate (mL·min <sup>-1</sup> ·g <sup>-1</sup> )	The total volume of H <sub>2</sub> (mL)	Time (min)
Ni	45	50.1	70
Co	50	50	66
Cu	70	50	58
Ni <sub>1</sub> Co <sub>3</sub>	250	43.8	35
Ni <sub>1</sub> Co <sub>2</sub>	546	49.1	18
Ni <sub>1</sub> Co <sub>1</sub>	364	49.2	27
Ni <sub>2</sub> Co <sub>1</sub>	327	49.0	30
Ni <sub>3</sub> Co <sub>1</sub>	316	49.0	31
Ni <sub>1</sub> Cu <sub>3</sub>	255	40.8	31
Ni <sub>1</sub> Cu <sub>2</sub>	517	49.1	19
Ni <sub>1</sub> Cu <sub>1</sub>	341	47.8	28
Ni <sub>2</sub> Cu <sub>1</sub>	347	48.6	28
Ni <sub>3</sub> Cu <sub>1</sub>	323	48.5	30
Co <sub>1</sub> Cu <sub>3</sub>	184	41.4	45
Co <sub>1</sub> Cu <sub>2</sub>	416	50.0	24
Co <sub>1</sub> Cu <sub>1</sub>	407	40.0	45
Co <sub>2</sub> Cu <sub>1</sub>	218	50.9	25
Co <sub>3</sub> Cu <sub>1</sub>	152	34.3	45
Ni <sub>1</sub> Co <sub>1</sub> Cu <sub>1</sub>	418	0.2	24
Ni <sub>2</sub> Co <sub>1</sub> Cu <sub>1</sub>	245	39.2	32
Ni <sub>1</sub> Co <sub>2</sub> Cu <sub>1</sub>	311	49.7	30
Ni <sub>1</sub> Co <sub>1</sub> Cu <sub>2</sub>	600	50.8	17

confirming the synergistic interactions inside the trimetallic NPs. On the other hand, the monometallic Ni, Co, and Cu NPs manifested low catalytic activity. Increasing the ratio of Cu, the reaction time decreased clearly below 15 min when the value was 0.4, which is Ni<sub>0.3</sub>Co<sub>0.3</sub>Cu<sub>0.4</sub>/TiO<sub>2</sub> sample. The maximum hydrogen generation rate was 600 mL·min<sup>-1</sup>·g<sup>-1</sup> obtained over Ni<sub>0.3</sub>Co<sub>0.3</sub>Cu<sub>0.4</sub>/TiO<sub>2</sub> as catalyst at 298 K. The catalytic performance changed in line with the variation of the amounts of Ni, Co, and Cu. Therefore, when the feed molar ratio of Cu:Co:Ni was 1:1:2 (i.e., Ni<sub>0.3</sub>Co<sub>0.3</sub>Cu<sub>0.4</sub>/TiO<sub>2</sub> catalyst), the best performance in the hydrolysis of AB without light irradiation was obtained.

The hydrogen generation rate, total H<sub>2</sub> volume, and reaction time for various catalysts without light irradiation are summarized in Table 1. The rate of hydrogen generation of Ni<sub>0.3</sub>Co<sub>0.3</sub>Cu<sub>0.4</sub>/TiO<sub>2</sub> is nearly 600 mL·min<sup>-1</sup>·g<sup>-1</sup>. This value is much higher than those obtained for the mono- and bimetallic NPs (i.e., Ni<sub>x</sub>Cu<sub>y</sub> and Co<sub>x</sub>Cu<sub>y</sub>), and also higher than those calculated for other trimetallic catalysts prepared in this work.

**Table 2** – The hydrogen generation rates of the AB hydrolysis of over bi- and trimetallic M/TiO<sub>2</sub> catalysts with UV-light assistance.

Catalyst	The rate (mL·min <sup>-1</sup> ·g <sup>-1</sup> )	The total volume of H <sub>2</sub> (mL)	Time (min)
Ni <sub>1</sub> Co <sub>2</sub>	827	49.6	12
Ni <sub>1</sub> Cu <sub>2</sub>	766	49.8	13
Co <sub>1</sub> Cu <sub>2</sub>	661	49.6	15
Ni <sub>0.3</sub> Co <sub>0.3</sub> Cu <sub>0.4</sub>	985	50.0	11

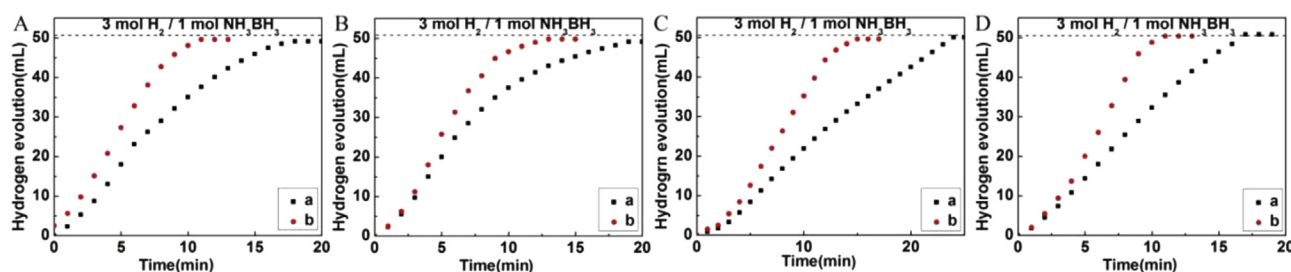
Hydrogen evolution without (dot a in the Fig. 6) and with (dot b in the Fig. 6) UV-light irradiation using different catalysts are shown in Fig. 6. It can be seen that the UV-light irradiation plays a great role for increasing the rate of hydrogen evolution. Table 2 shows the hydrogen generation rate, total H<sub>2</sub> volume, and reaction time for various catalysts with light irradiation. The rate of hydrogen generation of Ni<sub>0.3</sub>Co<sub>0.3</sub>Cu<sub>0.4</sub>/TiO<sub>2</sub> under light irradiation is nearly 985 mL·min<sup>-1</sup>·g<sup>-1</sup>. This value is superior to those obtained for the bimetallic catalysts with initial raw material molar ratio of Ni:Cu = 1:2 and Co:Cu = 1:2 under UV-light irradiation.

Fig. 7A–C show the hydrogen evolution over time at different temperatures (25, 30, 35, and 40 °C), Arrhenius, and Eyring plots, respectively. The slope of the straight line obtained by plotting lnk versus the reciprocal absolute temperature (1/T) was -7391, which gives an E<sub>a</sub> of 61.4 kJ·mol<sup>-1</sup>, according to Eq. (3). This value was lower than that previously reported (70 kJ·mol<sup>-1</sup>) for Ni [29] and a slightly lower than that of Co (62 kJ·mol<sup>-1</sup>) [29]. However, it is higher than that for Cu-RGO (38.2 kJ·mol<sup>-1</sup>) [30], which can be attributed to the support that is known to influence the value of E<sub>a</sub>. Fig. 7C illustrates the ln(k/T) vs 1/T graph for the Eyring equation (Eq. (4)). As can be seen in Fig. 7C, the Eyring equations fitted very well the data of the hydrolysis of AB over Ni<sub>0.3</sub>Co<sub>0.3</sub>Cu<sub>0.4</sub>/TiO<sub>2</sub> catalyst. The slope of the straight line was -7089 while the intercept was 14.86. The enthalpy and entropy for the AB hydrolysis catalyzed by Ni<sub>0.3</sub>Co<sub>0.3</sub>Cu<sub>0.4</sub>/TiO<sub>2</sub> were 58.9 and 45.12 J·mol<sup>-1</sup>·K<sup>-1</sup>, respectively, calculated according to Eq. (4).

$$\ln k = \ln A - E_a/RT \quad (3)$$

$$\ln(k/T) = \ln(kB/h) + (\Delta S/R) - (\Delta H/R) \times (1/T) \quad (4)$$

The recycling capability and durability are very important aspects for the practical applications of a catalyst in hydrogen

**Fig. 6** – Hydrogen evolution without (a) and with (b) UV-light assistance using different catalysts. A - Ni<sub>1</sub>Co<sub>2</sub>/TiO<sub>2</sub>, B - Ni<sub>1</sub>Cu<sub>2</sub>/TiO<sub>2</sub>, C - Co<sub>1</sub>Cu<sub>2</sub>/TiO<sub>2</sub>, D - Ni<sub>0.3</sub>Co<sub>0.3</sub>Cu<sub>0.4</sub>/TiO<sub>2</sub>.

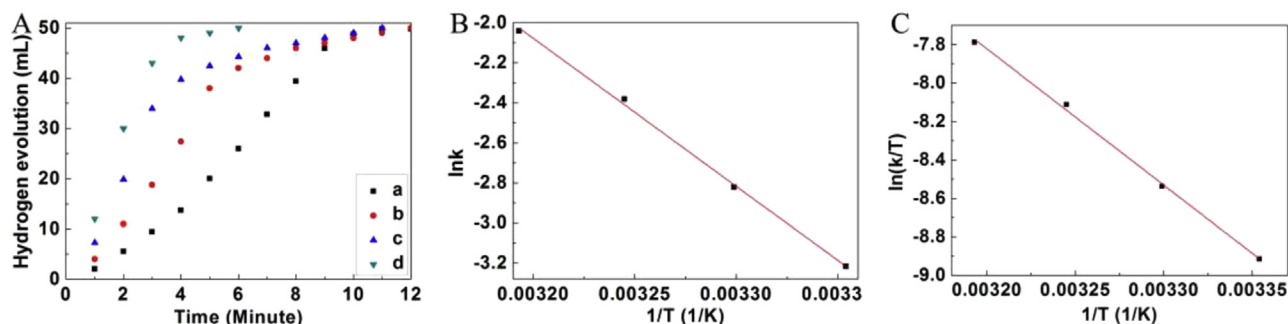


Fig. 7 –  $\text{H}_2$  released during the AB hydrolysis catalyzed by  $\text{Ni}_{0.3}\text{Co}_{0.3}\text{Cu}_{0.4}/\text{TiO}_2$  at different temperatures (25, 30, 35, and 40 °C). (A), the linear fitting of Arrhenius equation (B), and linear fitting of Eyring equation for the (C).

generation process. The prepared catalysts can be easily reused after recovering from the reaction medium and rinsing with distilled water without any other complex post-treatment steps while the catalytic efficiency is maintained at almost the same level as for the fresh catalyst, after each cycle. The recycling performance of the prepared catalysts is shown in Fig. 8. The hydrogen generation rate slightly decreased with the number of cycles, although it was still of  $714.3 \text{ mL}\cdot\text{min}^{-1}\cdot\text{g}^{-1}$  after 5 cycles. The rate of hydrolysis decreased after using for 5 times, results that can be explained by the cracks on the catalysts surface (Fig. 2c). The cracks observed on the surface indicate that the  $\text{TiO}_2$  spheres suffer fracture after the hydrolysis reaction. It is taught that this partial damage of the structure collapse weakens the metal-support interactions and thereby reduces the rate of reaction.  $\text{Ni}_{0.3}\text{Co}_{0.3}\text{Cu}_{0.4}/\text{TiO}_2$  retained 73% of its initial catalytic activity toward the hydrolysis of AB after 5 cycles, thereby showing a good stability of the catalyst. This value was significantly larger than that of  $\text{NiCo-GO}$  (ca. 65% after 3 cycles) reported by J. Zhong et al. [31], and also higher than that of  $\text{Cu}_{0.4}@_{\text{Co}_{0.5}\text{Ni}_{0.1}}$  core-shell nanoparticles (lower than 60% after 5 cycles) [32]. Although the hydrogen evolution rates obtained in this work were lower than those of other metal catalysts, the  $\text{Ni}_{0.3}\text{Co}_{0.3}\text{Cu}_{0.4}/\text{TiO}_2$  catalyst showed very promising recycle

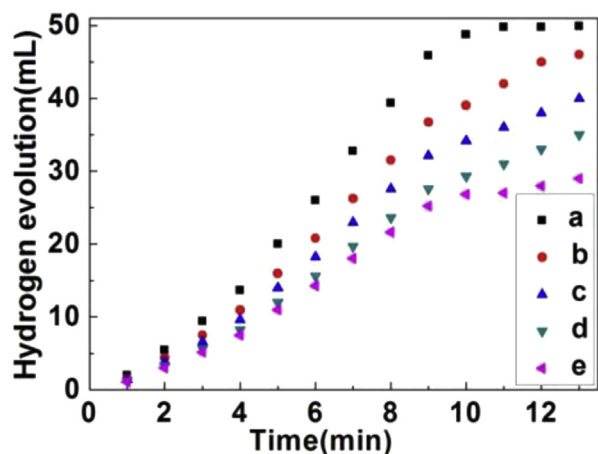


Fig. 8 –  $\text{H}_2$  released from AB hydrolysis catalyzed by  $\text{Ni}_{0.3}\text{Co}_{0.3}\text{Cu}_{0.4}/\text{TiO}_2$  (10 wt%) at 298 K for 5 cycles of reaction.

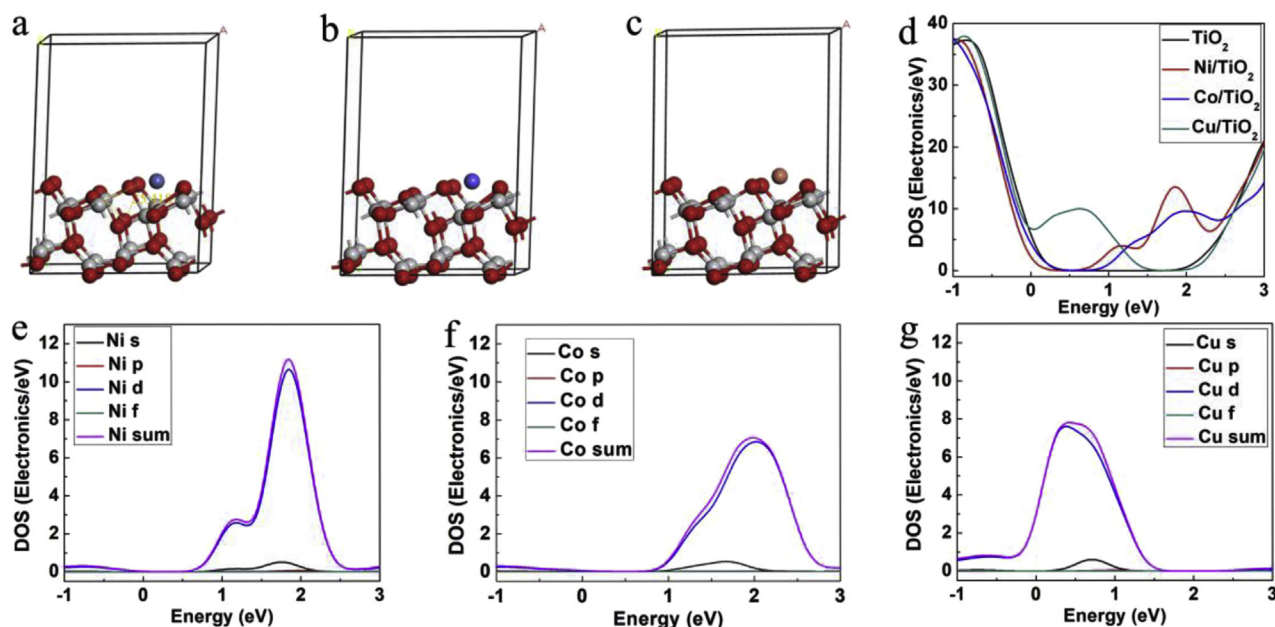
performance. The catalytic properties and recycle performance of the samples prepared herein was compared with those obtained for other non-noble catalysts reported so far in the literature. The values, those of TOF (turnover frequency) included, are summarized in the Table 3. It can be observed that the rate of reaction obtained when  $\text{Ni}_{0.3}\text{Co}_{0.3}\text{Cu}_{0.4}/\text{TiO}_2$  sample was used as catalyst is low, while the recycle performance is in line with that manifested by other catalysts.

#### Theoretical calculation

For the modeling studies, Ni, Co, or Cu adsorption on  $\text{TiO}_2$  (101) plane as a representative material of the catalysts was used. The optimized structures are displayed in Fig. 9a–c. The most stable sites are chosen according to a previous study [37], where M (M = Ni, Co, Cu) is directly bonded to two surface atoms, notably a three-fold oxygen ( $\text{O}_{3c}$ ) and a two-fold oxygen ( $\text{O}_{2c}$ ), with M–O bond distances of 2.57, 2.58, and 2.63 Å, respectively. The adsorption energy is large,  $-0.89$ ,  $-0.84$ , and  $-0.79$  eV, indicating a strong metal-support interaction. Fig. 9d shows the total density of states (TDOS) of pure  $\text{TiO}_2$  and M/ $\text{TiO}_2$ . It can be seen that no defect states occurred in the band gap of pure  $\text{TiO}_2$ . The new defect states in Ni, Co, or Cu supported  $\text{TiO}_2$  have been observed that was introduced by the d-orbitals of Ni, Co, Cu [38]. It can be seen that the d-orbitals of Ni, Co, Cu could hybridize with the intrinsic defect states to generate more states in band gap according to the partial density of states (pdos) shown in Fig. 9a–c. It can be observed from the pdos curves (Fig. 9e–g) that a small energy level near the conduction band minimum (CBM) is generated after including Ni, Co, or Cu into  $\text{TiO}_2$  model accompanied by a reduced band gap. After introducing Ni, Co, or Cu into  $\text{TiO}_2$ , some mid-gap states localized between the valence band maximum (VBM) and CBM can be observed in the DOS of composite catalytic materials. These results support the idea of the SMSI effect between the non-noble metals and  $\text{TiO}_2$ . In this case, when these catalysts are irradiated under visible light, the electrons excited can transfer from VB of M/ $\text{TiO}_2$  to these mid-levels or from one mid-level to CB of M/ $\text{TiO}_2$  easily. Meanwhile, the generated electrons in the CB of M/ $\text{TiO}_2$  are more difficult to move back from CB to VB, which prevents the corresponding recombination more efficiently [39]. This helps to improve the photocatalytic performance of M/ $\text{TiO}_2$ .

**Table 3 – Catalytic performance of different catalysts reported for AB hydrolysis.**

Catalyst	The rate ( $\text{mL} \cdot \text{min}^{-1} \cdot \text{g}^{-1}$ )	TOF ( $\text{mol H}_2 \cdot \text{min}^{-1} \cdot (\text{mol cat})^{-1}$ )	Re-usability (Retained rate after 5 cycles)	Ref.
Ag@CoFe/graphene	–	82.9	59%	[33]
$\text{Co}_{0.9}\text{Ni}_{0.1}$ /graphene	–	16.4	44%	[34]
p (AMPS)-Co:Ni	–	49	79%	[35]
$\text{Co}_{0.52}\text{Cu}_{0.48}$	2179	3.4	66%	[25]
$\text{Ni}_{0.19}\text{Cu}_{0.81}$	2066	2.7	61%	[25]
$\text{Cu}_{0.3}@\text{Fe}_{0.6}\text{Co}_{0.1}$	1211	–	43%	[36]
$\text{Cu}_{0.6}\text{Ni}_{0.4}\text{Co}_2\text{O}_4$	119.5	–	70%	[28]
$\text{Ni}_{0.3}\text{Co}_{0.3}\text{Cu}_{0.4}$	985	1.1	73%	This work

**Fig. 9 – Calculated models for Ni-TiO<sub>2</sub> (a), Co-TiO<sub>2</sub> (b), and Cu-TiO<sub>2</sub> (c), total density of state of pure TiO<sub>2</sub>, Ni-TiO<sub>2</sub>, Co-TiO<sub>2</sub> and Cu-TiO<sub>2</sub> (d), partial dos of Ni, Co, Cu support on TiO<sub>2</sub> (e–g).**

## Conclusion

$\text{Ni}_{0.3}\text{Co}_{0.3}\text{Cu}_{0.4}/\text{TiO}_2$  composite nanocatalyst was synthesized in a two-step process by in situ reduction. As catalyst for hydrogen generation by AB hydrolysis, the trimetallic NPs showed superior performance than mono- and bimetallic counterparts. The synergistic interaction between Ni, Co, and Cu may have played a critical role in the enhanced catalytic activity. Under UV-light irradiation,  $\text{Ni}_{0.3}\text{Co}_{0.3}\text{Cu}_{0.4}/\text{TiO}_2$  (10 wt %) as the catalyst can realize complete hydrolysis of ammonia borane in 10 min with an apparent activation energy of  $61.4 \text{ kJ} \cdot \text{mol}^{-1}$ . The roles of Ni, Co, Cu and TiO<sub>2</sub> in the hydrolysis with UV-light irradiation were evaluated by Dmol<sup>3</sup> to explain the SMSI between metallic NPs and TiO<sub>2</sub> support. Moreover, the  $\text{Ni}_{0.3}\text{Co}_{0.3}\text{Cu}_{0.4}/\text{TiO}_2$  catalyst manifested good reusability, 78% of original catalytic activity being maintained after 5 catalytic runs. These results indicate  $\text{Ni}_{0.3}\text{Co}_{0.3}\text{Cu}_{0.4}/\text{TiO}_2$  nanocomposite as a performance catalyst for the hydrolysis of AB.

## Acknowledgments

This work was supported by the National Natural Science Foundation of China (No. 21603052, 51771068 and 51771067), Natural Science Foundation of Hebei Province (No. B201820167).

## REFERENCES

- [1] Chen JQ, Hu M, Ming M, Xu CL, Wang Y, Zhang Y, et al. Carbon-supported small Rh nanoparticles prepared with sodium citrate: toward high catalytic activity for hydrogen evolution from ammonia borane hydrolysis. *Int J Hydrogen Energy* 2018;43:2718–25.
- [2] Cao ZJ, Ou Yang LZ, Li LL, Lu YS, Wang H, Liu JW, et al. Enhanced discharge capacity and cycling properties in high-samarium, praseodymium/neodymium-free, and low cobalt

- $A_2B_7$  electrode materials for nickel-metal hydride battery. *Int J Hydrogen Energy* 2015;40:451–5.
- [3] Liu Y, Guan HJ, Zhang J, Zhao YF, Yang JH, Zhang B. Polydopamine-coated halloysite nanotubes supported AgPd nanoalloy: an efficient catalyst for hydrolysis of ammonia borane. *Int J Hydrogen Energy* 2018;43:2754–62.
- [4] Wright WRH, Berkeley ER, Alden LR, Baker RT, Sneddon LG. Transition metal catalysed ammonia-borane dehydrogenation in ionic liquids. *Chem Commun* 2011;47:3177–9.
- [5] Diwan M, Diakov V, Shafirovich E, Varma A. Noncatalytic hydrothermolysis of ammonia borane. *Int J Hydrogen Energy* 2008;33:1135–41.
- [6] Zahmakiran M, Durap F, Szkar Ö. Zeolite confined copper(0) nanoclusters as cost-effective and reusable catalyst in hydrogen generation from the hydrolysis of ammonia-borane. *Int J Hydrogen Energy* 2010;35:187–97.
- [7] Bluhm ME, Bradley MG, Butterick R, Kusari U, Sneddon LG. Amine borane-based chemical hydrogen storage: enhanced ammonia borane dehydrogenation in ionic liquids. *J Am Chem Soc* 2006;128:7748–9.
- [8] Fan GY, Liu QQ, Tang DM, Li XJ, Bi J, Gao DJ. Nanodiamond supported Ru nanoparticles as an effective catalyst for hydrogen evolution from hydrolysis of ammonia borane. *Int J Hydrogen Energy* 2016;41:1542–9.
- [9] Xu CL, Hu M, Wang Q, Fan GY, Wang Y, Zhang Y, et al. Hyper-cross-linked polymer supported rhodium: an effective catalyst for hydrogen evolution from ammonia borane. *Dalton Trans* 2018;47:2561–7.
- [10] Lu R, Hu M, Xu CL, Wang Y, Zhang Y, Xu B, et al. Hydrogen evolution from hydrolysis of ammonia borane catalyzed by Rh/g- $C_3N_4$  under mild conditions. *Int J Hydrogen Energy* 2018;43:7038–45.
- [11] Yao QL, Lu ZH, Zhang ZJ, Chen XS, Lan YQ. One-pot synthesis of core-shell Cu@SiO<sub>2</sub> nanospheres and their catalysis for hydrolytic dehydrogenation of ammonia borane and hydrazine borane. *Sci Rep* 2014;4:7597–605.
- [12] Yao QL, Lu ZH, Huang W, Chen XS, Zhu J. Highly Pt-like activity of Ni-Mo/graphene catalyst for hydrogen evolution from hydrolysis of ammonia borane. *J Mater Chem A* 2016;4:8579–83.
- [13] Yao QL, Yang K, Hong XL, Chen XS, Lu ZH. Base-promoted hydrolytic dehydrogenation of ammonia borane catalyzed by noble-metal-free nanoparticles. *Catal Sci Technol* 2018;8:870–7.
- [14] Yan JM, Zhang XB, Han S, H SY, Xu Q. Iron-nanoparticle-catalyzed hydrolytic dehydrogenation of ammonia borane for chemical hydrogen storage. *Angew Chem Int Ed* 2008;47:2287–9.
- [15] Sahiner N, Ozay O, Inger E, Aktas N. Superabsorbent hydrogels for cobalt nanoparticle synthesis and hydrogen production from hydrolysis of sodium boron hydride. *Appl Catal B* 2011;102:201–6.
- [16] Wang HL, Yan JM, Wang ZL, Jiang Q. One-step synthesis of Cu@FeNi core-shell nanoparticles: highly active catalyst for hydrolytic dehydrogenation of ammonia borane. *Int J Hydrogen Energy* 2012;37:10229–35.
- [17] Shen XC, Dai M, Gao M, Wang ZB, Zhao B, Ding WP. Synthesis and catalytic performance for hydrolysis of ammonia borane aqueous solution. *Chin J Inorg Chem* 2013;29:999–1006.
- [18] Dai M, Shen XC, Wang Q, Wang ZB, Zhao B, Ding WP. Synthesis of Core/Shell structured Cu@CoW catalysts and its catalytic properties for hydrolysis of ammonia borane aqueous solution. *Chin J Inorg Chem* 2014;10:2375–81.
- [19] Jia Y, Han W, Xiong G, Yang W. Layer-by-layer assembly of TiO<sub>2</sub> colloids onto diatomite to build hierarchical porous materials. *J Colloid Interface Sci* 2008;323:326–31.
- [20] Rakap M, Kalu EE, Zkar SO. Polymer-immobilized palladium supported on TiO<sub>2</sub> (Pd-PVB-TiO<sub>2</sub>) as highly active and reusable catalyst for hydrogen generation from the hydrolysis of unstirred ammonia-borane solution. *Int J Hydrogen Energy* 2011;36:1448–55.
- [21] Yousef A, Halwany MME, Barakat NAM, Kim HY. One pot synthesis of Cu-doped TiO<sub>2</sub> carbon nanofibers for dehydrogenation of ammonia borane. *Ceram Int* 2015;41:6137–40.
- [22] Pant B, Pant HR, Park M, Liu YN, Choi JW, Barakat NAM, et al. Electrospun CdS–TiO<sub>2</sub> doped carbon nanofibers for visible-light-induced photocatalytic hydrolysis of ammonia borane. *Catal Commun* 2014;50:63–8.
- [23] Yousef A, Barakat NAM, Kim HY. Electrospun Cu-doped titania nanofibers for photocatalytic hydrolysis of ammonia borane. *Appl Catal A: Gen* 2013;467:98–106.
- [24] Deng Z, Chen M, Zhou S, You B, Wu L. A novel method for the fabrication of monodisperse hollow silica spheres. *Langmuir* 2006;22:6403–7.
- [25] Sang WL, Wang CY, Zhang XH, Yu XF, Yu C, Zhao JL, et al. Dendritic Co<sub>0.52</sub>Cu<sub>0.48</sub> and Ni<sub>0.15</sub>Cu<sub>0.85</sub> alloys as hydrogen generation catalysts via hydrolysis of ammonia borane. *Int J Hydrogen Energy* 2017;42:30691–703.
- [26] Li LL, Yang SQ, Yang XJ, Xu XW, Tang CC. Boron adsorption induced magnetism in zigzag boron nitride nanotubes. *J Mol Struct* 2012;1020:183–7.
- [27] Perdew JP, Wang Y. Accurate and simple analytic representation of the electron-gas correlation energy. *Phys Rev B* 1992;45:13244–9.
- [28] Lu DS, Liao JY, Zhong SD, Leng Y, Ji S, Wang H, et al. Cu<sub>0.6</sub>Ni<sub>0.4</sub>Co<sub>2</sub>O<sub>4</sub> nanowires, a novel noble-metal free catalyst with ultrahigh catalytic activity towards the hydrolysis of ammonia borane for hydrogen production. *Int J Hydrogen Energy* 2018;43:5541–50.
- [29] Yang XJ, Li LL, Sang WL, Zhao JL, Wang XX, Yu C, et al. Boron nitride supported Ni nanoparticles as catalysts for hydrogen generation from hydrolysis of ammonia borane. *J Alloy Compd* 2017;693:642–9.
- [30] Yang YW, Lu ZH, Hu YJ, Zhang ZJ, Shi WM, Chen XS, et al. Facile in situ synthesis of copper nanoparticles supported on graphene for hydrolytic dehydrogenation of ammonia borane. *RSC Adv* 2014;4:13749–52.
- [31] Zhao BH, Liu JY, Zhou LT, Long D, Feng K, Sun XH, et al. Probing the electronic structure of M-graphene oxide (M=Ni, Co, NiCo) catalysts for hydrolytic dehydrogenation of ammonia borane. *Appl Surf Sci* 2016;362:79–85.
- [32] Zhang H, Wang XF, Chen CC, An CH, Xu YN, Huang YA, et al. Facile synthesis of Cu@CoNi core-shell nanoparticles composites for the catalytic hydrolysis of ammonia borane. *Int J Hydrogen Energy* 2015;40:12253–61.
- [33] Yang L, Su J, Luo W, Cheng GZ. Strategic synthesis of graphene supported trimetallic Ag-based core-shell nanoparticles toward hydrolytic dehydrogenation of amine boranes. *Int J Hydrogen Energy* 2014;39:3360–70.
- [34] Feng WQ, Yang L, Cao N, Du C, Dai HG, Luo W, et al. In situ facile synthesis of bimetallic CoNi catalyst supported on graphene for hydrolytic dehydrogenation of amine borane. *Int J Hydrogen Energy* 2014;39:3371–80.
- [35] Nurettin S, Ozgur O, Nahit A, Erk I, Jibao H. The on demand generation of hydrogen from Co-Ni bimetallic nano catalyst prepared by dual use of hydrogel: as template and as reactor. *Int J Hydrogen Energy* 2011;36:15250–8.

- [36] Qiu FY, Da YL, Li L, Xu CC, Huang YA. Synthesis of Cu@FeCo core-shell nanoparticles for the catalytic hydrolysis of ammonia borane. *Int J Hydrogen Energy* 2014;39:436–41.
- [37] Wang HH, An TC, Selloni A. Effect of reducible oxide–metal cluster charge transfer on the structure and reactivity of adsorbed Au and Pt atoms and clusters on anatase TiO<sub>2</sub>. *J Chem Phys* 2017;146:184703–11.
- [38] Park MS, Kwon SK, Min BI. Electronic structures of doped anatase TiO<sub>2</sub>:Ti<sub>1-x</sub>M<sub>x</sub>O<sub>2</sub> (M = Co Mn, Fe, Ni). *Phys Rev B* 2002;65:161201.
- [39] Yang NL, Liu YY, Wen H, Tang Z, Zhao H, Li YL, et al. Photocatalytic properties of graphdiyne and graphene modified TiO<sub>2</sub>: from theory to experiment. *ACS Nano* 2013;7:1504.